Intramolecular H-atom transfer reactions in rigid peptides — Correlated solvent and structural effects

Anna Lewandowska, Gordon L. Hug, Gerald Hörner, Dariusz Pogocki, Franciszek Kazmierczak, and Bronislaw Marciniak

Abstract: The rates and the mechanism of intramolecular hydrogen-atom transfer across the rigid diketopiperazine spacer in two epimeric benzophenone–tyrosine dyads were studied by nanosecond laser flash photolysis in 12 non-protic and protic solvents. Effects of the stereochemistry on the ground-state structures and conformational equilibria and dynamics have been addressed by means of NMR-based population analysis and long-term molecular-dynamics simulations. The excited triplet state of the benzophenone is found to be quenched intramolecularly by the remote phenol moiety with rates that are highly dependent on the solvent and on the relative benzophenone–phenol orientation. In agreement with previous studies, the kinetic diversity, with rates ranging from $<10^5$ s^{-1} to 2×10^7 s^{-1}, can be attributed to retarding effects of the bulk viscosity and to effects of specific solvation, which can be both rate retarding and rate accelerating. As an extension of the previous knowledge, however, the phenomenology of the kinetic solvent effects, that is, the nature of the predominating solvent parameter and its absolute impact on the reactivity, is found to be highly correlated with structural effects.

Key words: kinetic solvent effect, stereoselectivity, biradicals, tyrosyl radical, molecular dynamics.

Résumé : Utilisant la photolyse laser éclair, au niveau de la nanoseconde, on a étudié les vitesses et le mécanisme de réaction du transfert d'atome d'hydrogène intramoléculaire à travers l'espaceur dicétopipérazine rigide dans deux dyades de benzophénone–tyrosine dans douze solvants protiques et aprotiques. Faisant appel à l'analyse de populations à l'aide de la RMN et de simulations de dynamique moléculaire à long terme, on a étudié les effets de la stéréochimie sur les structures de l'état fondamental et sur la dynamique et les équilibres conformationnels. On a trouvé que l'état triplet excité de la benzophénone est piégé d'une façon intramoléculaire par la portion phénolique éloignée avec des vitesses qui dépendent beaucoup du solvant et des orientations relatives de la benzophénone et du phénol. En accord avec les études antérieures, la diversité cinétique des vitesses qui varient de moins de 10^5 s^{-1} à 2×10^7 s^{-1} peut être attribuée aux effets de viscosité globale qui les diminuent et aux effets de solvatation spécifique qui peuvent soit les accélérer ou les retarder. Toutefois, comme extension aux connaissances acquises antérieurement, on a trouvé que la phénoménologie des effets cinétiques du solvant, c'est-à-dire la nature du paramètre prédominant du solvant et son impact absolu sur la réactivité, est intimement reliée aux effets structuraux.

Mots-clés : effet cinétique du solvant, stéréosélectivité, biradicaux, radical tyrosyle, dynamique moléculaire.

[Traduit par la Rédaction]

Introduction

Photoinduced hydrogen-abstraction reactions by triplet-excited carbonyl compounds have been a central topic of photochemical research for many years.[1] Starting off with the seminal study by Das and Scaiano in 1981,[2] the reactions of phenols with triplet-excited carbonyl compounds have stimulated recurrent interest.[3–26] Hydrogen-atom transfer (HAT) from the phenol to the excited carbonyl provides, quite invariantly with respect to the nature of the carbonyl compound, an efficient source of metastable radicals, namely the carbonyl-derived ketyl radical and the phenoxyl

Received 29 April 2010. Accepted 30 June 2010. Published on the NRC Research Press Web site at canjchem.nrc.ca on 15 February 2011.

This article is part of a Special Issue dedicated to Professor J. C. Scaiano.

A. Lewandowska, F. Kazmierczak, and B. Marciniak.[2] Faculty of Chemistry, Adam Mickiewicz University, 60-780 Poznan, Poland.
G.L. Hug. Faculty of Chemistry, Adam Mickiewicz University, 60-780 Poznan, Poland; Radiation Laboratory, University of Notre Dame, Notre Dame, IN 46556, USA.
G. Hörner.[1] Faculty of Chemistry, Adam Mickiewicz University, 60-780 Poznan, Poland; Institut für Chemie, Technische Universität Berlin, 10623 Berlin, Germany.
D. Pogocki. Faculty of Biology and Agriculture, University of Rzeszow, 35-601 Rzeszow, Poland; Centre of Radiation Research and Technology, Institute of Nuclear Chemistry and Technology, 03-195 Warsaw, Poland.

[1]Corresponding author (e-mail: hoerner@amu.edu.pl).
[2]Corresponding author (e-mail: marcinia@amu.edu.pl).

radical. Ample use of these clean radical-affording pathways has allowed the selective formation and the characterization of biologically relevant phenoxyl radicals that are derived, for instance, from the phenolic amino acid tyrosine (Tyr)[7] and from the phenolic neurotransmitter adrenaline.[6] Selective generation of fluorinated tyrosyl radicals within biological matrices has allowed their use as a mechanistic probe and as an external trigger of proton-coupled electron transfer reactions in native proteins.[27]

This biochemical application was based on an intramolecular variation of the carbonyl–phenol theme within covalently bound dyads. Mechanistic studies of the intramolecular HAT pathways corroborated the view that such dyads share the reaction pathways with their bimolecular congeners and, thus, produce the corresponding biradicals with high selectivity and efficiency as long as the structural constraints of the dyad allow close contacts between the reacting moieties. The intramolecular HAT quenching of, for instance, the benzophenone triplet state (^{3}bp) by an H-atom donor, RH, implies that >C=O···HR distances below 3.1 Å are successful.[28] Studies of the intramolecular HAT of several benzophenone-based dyads have provided evidence that the chemical nature of the linker between the chromophores (that is, the flexibility and the directionality of the linker) is one major source of kinetic diversity. Remarkable variations in the reaction rates of isomeric benzophenone–phenol dyads (regiomers and stereomers) have been attributed to modulations of the distance distributions and relative orientations of the reacting moieties.[10,12,19]

In extension of previous work on the solvent effects of the intramolecular HAT by Scaiano, Miranda, Leigh, and others,[2,12,16,19,23] our recent systematic studies of the HAT reactions of peptide-linked benzophenone–tyrosine dyads (bp∪Tyr) have shown that this interpretation of structurally imposed kinetic effects is incomplete. Instead, specific solvent–solute interactions have been identified as the second important control of the intramolecular HAT dynamics.[29,30] Our results imply that the kinetic effects that are imposed by the solvent and those that are due to the dyad structure are correlated with each other and that they must not be treated separately. In non-protic solvents the intramolecular reactivity was generally found to be linearly correlated with the solvents' hydrogen-acceptor strength, which parallels the phenomenology of the solvent dependence of bimolecular HAT reactions of phenols.[31–36] In particular, the HAT reaction in two epimeric bp∪Tyr dyads exhibited significantly solvent-dependent stereoselectivity, which could be attributed to specific solvent–solute interactions.[29]

In the latter work the chromophores were connected by open-chain peptide structures (see Scheme 1; A denotes ^{3}bp as the hydrogen acceptor; HD denotes hydrogen donor PhOH), wherein the high intrinsic flexibility of the linker blurs the stereoselectivity. Therefore, limiting the flexibility of the peptide linker should allow deeper insights into the relations between the kinetic phenomenology and the molecular structure. The diketopiperazine (DKP) ring system provides such a peptide environment with reduced flexibility. First, the DKP ring imposes a distinct orientation between the reacting chromophores for epimeric dyads (see Scheme 1; from left to right, the structures denote the (L-L) and (L-D) epimers). In addition, the presence of the DKP ring exerts unique control over the conformations of the respective side chains of the attached amino acids. Previous studies of the conformations of substituted diketopiperazines revealed structural preferences that significantly differed from those of their open-chain analogues.[37,38] Such structural preferences are expected to be reflected in the nonbonding distances of the side chains and the inter-side-chain reactivity.

Preliminary work on the HAT between tyrosine and 4-benzoyl-phenylalanine (bpa) side chains of the epimeric diketopiperazines **1** and **2** (see Scheme 2*a*) actually showed significantly enhanced stereoselectivity.[39]

Herein, we present the results of extended laser-flash photolysis studies of **1** and **2** that address the medium dependence of the excited-state dynamics in more detail. These studies are supplemented by the results of molecular-dynamics simulations and NMR investigations of the ground-state structures and conformations that establish a quantitative picture of the conformer distributions of the dyads and define the molecular prerequisites of the individual quenching geometries. As will be shown, the presence of the rigid DKP linker imposes very different structural constraints on the intramolecular mobility of epimers **1** and **2**. These structural differences translate into individual phenomenology of the solvent effects for both of the dyads.

Experimental section

Synthesis and characterization

Chemicals and solvents (Sigma-Aldrich and BACHEM) for synthesis were of the highest available analytical grade and were used without further purification. Products were identified by means of NMR techniques and combustion analysis. Routine ^{1}H NMR and ^{13}C NMR spectra were recorded at 200/400 MHz and 50.3 MHz, respectively, in perdeuterated dimethyl sulfoxide (DMSO-d_6) and in deuterated trifluoroacetic acid (TFA-*d*), with the resonances being reported in parts per million downfield from tetramethylsilane. Assignments of ^{1}H and ^{13}C resonances were based on two-dimensional homo- and heteronuclear NMR techniques. An unambiguous assignment of the strongly overlapping β-proton resonances of the bpa and the Tyr residues in **1** and **2**, as required for the analysis of the ground-state rotamer distribution, was accomplished by two-dimensional nuclear Overhauser enhancement spectra (see Figs. S1 and S2 in the Supplementary data). The assignment of the $H^{\beta R}$ and $H^{\beta S}$ in the Tyr side chain of **1** and **2** as the high-field and the low-field doublet-of-doublet parts of the AB sub-spectrum, respectively, followed established conventions.[40] The same assignment was assumed to hold for the bpa side chain. The synthesis of the cyclic dipeptides (diketopiperazines, DKPs) **1** and **2** followed the method invented by Nitecki et al.[41] The fully protected open-chain precursors *N*-boc-(L/D)-bpa-(L)-Tyr-OMe were obtained by standard peptide-coupling methods as recently described in detail.[29] The cyclic peptides were obtained from the precursors after acidic deprotection of the N-terminus in formic acid followed by thermally

Scheme 1. Schematic of the structural constraints of the intramolecular H-atom transfer between a hydrogen donor (HD) and an acceptor (A) within linear and cyclic dipeptide scaffolds (asterisks denote chiral carbon centers; curved arrows (blue in the Web version) denote additional degrees of rotational freedom in the open-chain arrangements).

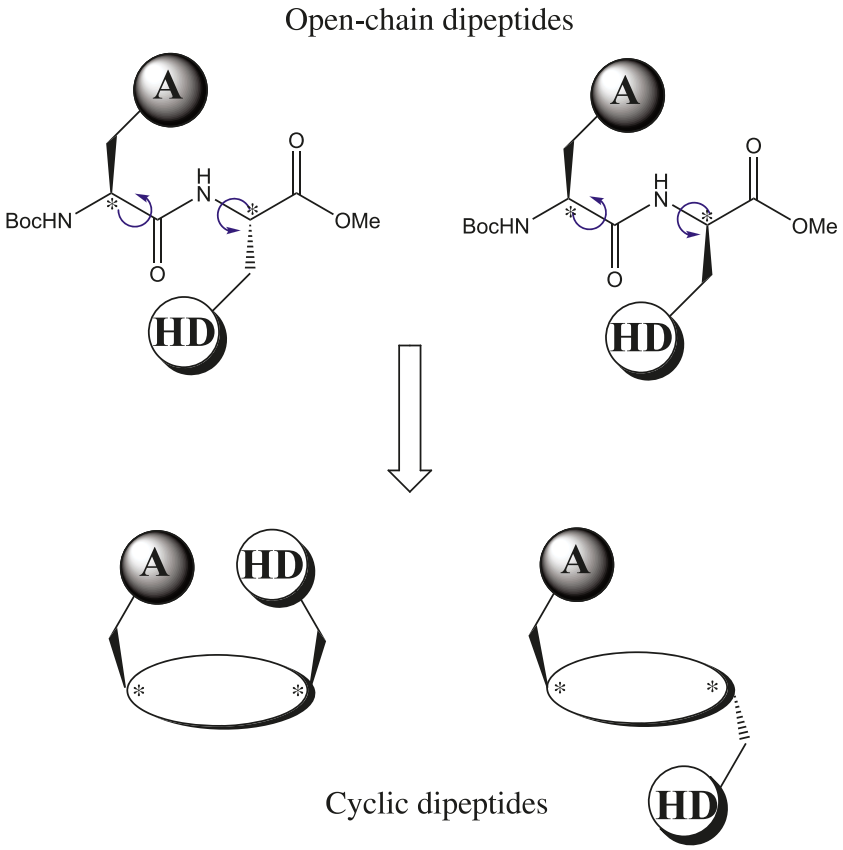

Scheme 2. (*a*) Structures of the diketopiperazines **1** and **2** and notation of atom positions; (*b*) notation of the side-chain rotamers for the L-configured side chains in **1** and **2** (R denotes the respective aromatic moiety); the D-configured bpa residue in dyad **1** is accounted for by an interchange of the >NH and >CO groups.

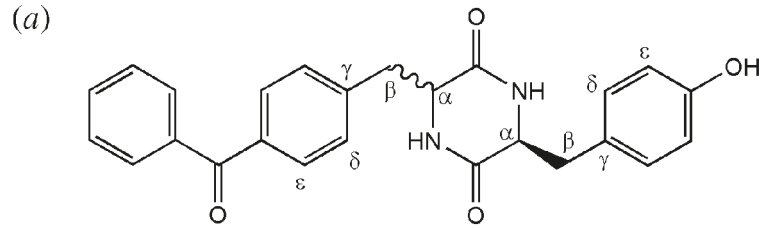

1 (*c*-(*D*)-bpa-(*L*)-Tyr)
2 (*c*-(*L*)-bpa-(*L*)-Tyr)

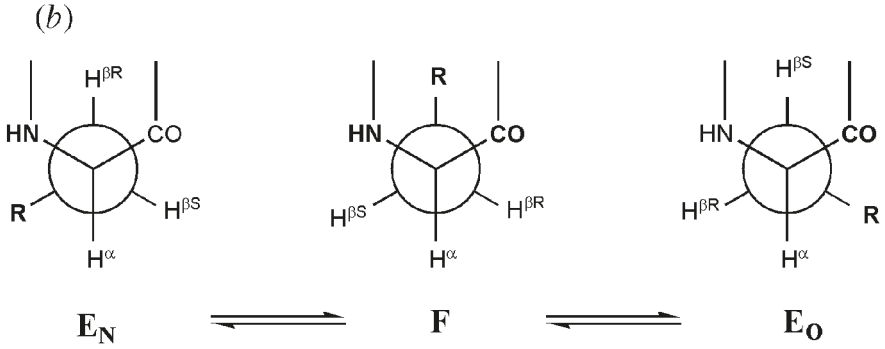

induced cyclization (full synthetic procedures and details of characterization are given in the Supplementary data).

Molecular modeling details

The conformational space of the DKPs **1** and **2** was sampled by means of Langevin dynamics (LD)[42–48] done in conjunction with the CHARMM27[49] all-atom empirical potential. Since there is no representation of the diphenylketone functionality in the original CHARMM force field, the parameters for the atoms of its aromatic rings were taken from the atoms of the phenylalanine residue. Similarly, the carbonyl oxygen and carbon atoms of the ketone functionality were calculated with parameters provided for these atoms in the peptide bond. To achieve consistency of charge distribution in the molecules, the atomic charges were recalculated using the partial equalization of orbital electronegativity method of Gasteiger and Marsili.[50] In the LD no explicit solvent molecules were used, but the usual LD frictional drag of the solvent was factored in using a collision frequency for all heavy atoms equal to approx. 20 ps^{-1}, which reflects the viscosity of acetonitrile, fitting molecular dynamics and experimental data.[44,51] The free LD simulations were done with the 2 fs time step and 100 ns propagation time, preceded by 12 ps of heating from 0 K to 300 K and 18 ps of equilibration. For the force field calculations we used version 7.1 of the HyperChem PC molecular modeling package,[52] which integrates the Langevin equation of motion using the method of Allen and Tildesley.[53]

The rate constants of the close-contact formation between the reacting moieties, here k_{OO}, have been evaluated from the simulations by means of number correlation functions, following the routines that have been described in detail previously.[54] If the reactive and non-reactive conformations are considered as being in equilibrium but the overall H-abstraction reaction is very fast compared with the relaxation of equilibrium between the conformations, then the observed rate constant k_H should be comparable to a theoretical rate constant, k_{OO}, computed from the simulation via eqs. [1–3].[54] The numerator, $\langle N_{OO}\rangle$, in eq. [1] is the fraction of the time that the distance between the carbonyl and hydroxyl oxygens was less than 4 Å during an 80 ns LD trajectory. The denominator, τ_{rxn}, in eq. [1] is the relaxation time for the equilibrium between the reactive and non-reactive conformations. It is related to a correlation function by the fluctuation-dissipation theorem.[55] The normalized number correlation function $C_N(t)$ was used for this calculation (see eq. [2]).

$$[1] \qquad k_{OO} = \frac{\langle N_{OO}\rangle}{\tau_{rxn}}$$

$$[2] \qquad \tau_{rxn} = \int_0^{+\infty} C_N(t)\,dt$$

which has the form

$$[3] \qquad C_N(t) = \frac{\langle \delta N_{OO}(t)\delta N_{OO}(0)\rangle}{\langle \delta N_{OO}{}^2\rangle}$$

Here $\delta N_{OO}(t) = N_{OO}(t) - \langle N_{OO}\rangle$ and $N_{OO}(t) = 1$ for $d_{OO} \leq 4.0$ Å and $N_{OO}(t) = 0$ for $d_{OO} \geq 4.0$ Å. Note that $\langle \delta N_{OO}{}^2\rangle = \langle N_{OO}\rangle - \langle N_{OO}\rangle^2$. The statistical error of the evaluation has been taken into account following the approach of Zwanzig and Ailawadi.[55,56]

Nanosecond flash photolysis

The setup for the nanosecond laser flash photolysis (LFP) experiments and the data acquisition system have been previously described in detail.[57,58] LFP experiments employed a pulsed N_2 laser (337 nm, 5 mJ, ≈8 ns) and a Nd:YAG laser (266 nm and 355 nm, 5 mJ, 7–9 ns) for excitation. Transient decays were recorded at individual wavelengths by the step-scan method with a step distance of 10 nm in the range of 320 to 700 nm as the mean of 10 pulses. Samples for LFP were deoxygenated with high-purity argon for 15 min prior to the measurements. Experiments were performed in rectangular quartz cells (1 cm × 1 cm). All experiments were performed with freshly prepared solutions at room temperature (295 ± 1 K). In the case of 266 nm photolysis, excitation of both chromophores (bp and Tyr) cannot be avoided. However, analysis of the molar absorption coefficients measured for bp and Tyr[59] shows that excitation of the tyrosine moiety was less than 10%. We used 266 nm excitation (which allowed us to use lower dyad concentrations) to avoid bimolecular hydrogen abstraction by the triplet state from the ground state of the dyad (self-quenching). Solvents for time-resolved spectroscopy were of the highest available analytical grade and were used without further purification.

Results

NMR study of ground-state conformations

A previous density functional theory (DFT) study of the DKPs **1** and **2** revealed the structural details of the respective quenching geometries and a qualitative interrelation between the inter-side-chain reactivity and structural preferences, which are reflected in the non-bonding distances of the side chains.[39] The cited work has shown that a variety of structures that differ in their relative side-chain orientations should be energetically accessible in solution. Therefore it was of interest to obtain quantitative information about the populations of the side-chain rotamers in the dyads' ground state. Herein we present the results of an NMR-based analysis of the absolute populations of the side-chain rotamers of the DKPs **1** and **2**. An important result is that the NMR-derived populations are distinctly different between the epimeric dyads **1** and **2**.

The populations of the rotamers $p(\boldsymbol{i})$ were extracted from the vicinal coupling constants of the diastereotopic β-protons and the α-protons of both of the amino-acid side chains, $^3J(H^{\alpha}–H^{\beta R})$ and $^3J(H^{\alpha}–H^{\beta S})$ (here bpa and Tyr; see Scheme 2*a* for the notation of the proton positions),[60] as recently used in the analysis of open-chain dyads.[29,30] The acronyms $\mathbf{E_N}$, $\mathbf{E_O}$, and **F** denote side-chain rotamers wherein the aromatic substituent R is extended to the adjacent nitrogen atom, extended to the adjacent carbonyl oxygen atom, and folded back across the DKP ring, respectively. This rotamer notation is based on the orientation of the side-chain substituent R (see Scheme 2*b*) rather than on the dihedral angles, to simplify the comparison between the epimeric compounds **1** and **2**. The computed rotamer populations for DMSO-d_6 and TFA-*d* are summarized in Table 1. The limited

Table 1. Summary of the side-chain rotamer populations $p(\boldsymbol{i})$ of the diketopiperazines **1** and **2** computed from experimental coupling constants (DMSO-d_6; 200 MHz).

	bpa residue			Tyr residue		
	$p(\mathbf{E_N})$	$p(\mathbf{E_O})$	$p(\mathbf{F})$	$p(\mathbf{E_N})$	$p(\mathbf{E_O})$	$p(\mathbf{F})$
1	0.22 (0.40)	0.10 (0.17)	0.68 (0.43)	0.18 (0.21)	0.07 (0.21)	0.75 (0.58)
2	0.42 (0.55)	0.20 (0.16)	0.38 (0.29)	0.26 (0.33)	0.20 (0.16)	0.54 (0.51)

Note: Estimated uncertainty $\Delta p(\boldsymbol{i}) = \pm 0.02$ and ± 0.04 for $p(\mathbf{E_N})$ ($p(\mathbf{E_O})$) and $p(\mathbf{F})$, respectively. Data in parentheses denote the populations in TFA-*d*.

Fig. 1. DFT minimized structures of highly populated solution-phase conformations of **1** (**F–F**) and **2** (**F–E$_N$**). (Note that the **1** shown here is the stereoisomer used in the LFP experiments, but the **1** shown in Scheme 2 is the stereoisomer used in the NMR and LD simulations. These two species, both labeled **1**, are identical molecules, being the mirror image of each other, and a limited set of duplicate LFP experiments verified their identical chemical behavior.)

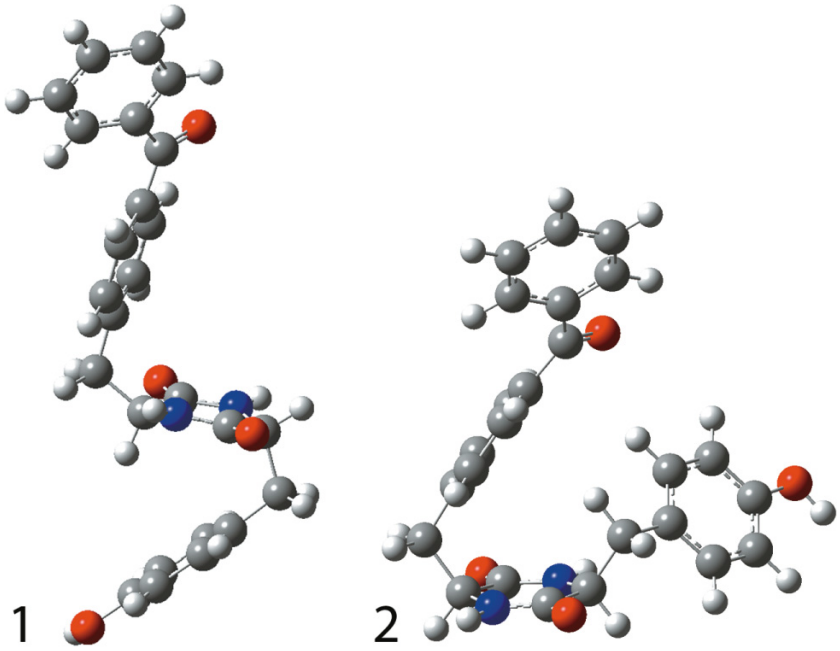

solubility of the DKPs under study interfered with a detailed investigation of the solvent dependence of the rotamer populations. It is noted that the population preferences of **1** and **2** are somewhat blurred in solutions of the very strong H-bond donor TFA.

The NMR-derived populations for DMSO solutions of **1** and **2** reveal side-chain conformational preferences that differ significantly from those of open-chain congeners. The aromatic side chains in linear peptides preferably populate the rotamer $\mathbf{E_N}$ in polar solvents such as DMSO, with $p(\mathbf{E_N}) \geq 0.7$.[61–64] In contrast, $\mathbf{E_N}$ appears to be much less favorable in the cyclic peptide **1**, where both aromatic residues preferably populate the back-folded **F** conformation instead. This behavior is quite common for the DKPs that carry aromatic amino acids and has been associated with dipole-induced dipole interactions between the DKP amides and the aromatic ring.[65,66] Based on the assumption that the conformer populations of the two side chains of **1** are statistically independent, a favored population of the **F–F** conformation can be expected with $p(\mathbf{F–F}) = 0.68 \times 0.75 = 0.51$. Thus, in full agreement with the outcomes of the previous DFT studies in an acetonitrile (ACN) continuum, a "double-sandwich" like structure of **1** also prevails in DMSO solution, which implies long inter-side-chain distances (see Fig. 1).

For **2**, wherein both aromatic residues share the same half-room above the DKP ring, the side-chain preferences are less expressed. When compared with dyad **1**, significantly smaller populations of the **F** conformation are obtained for **2**. In particular, the **F–F** conformation of **2** would contribute only with $p(\mathbf{F–F}) = 0.38 \times 0.54 = 0.20$, if statistically independent conformer populations can be reasonably assumed. In fact, the molecular-dynamics simulations show that this latter assumption is not valid for **2** and that even smaller populations prevail (vide infra). This finding of diminished populations of **F–F** is important for the interpretation of the excited-state dynamics of **2**, because photoinduced HAT within **2** is limited to the **F–F** conformation of the side chains wherein both aromatic moieties are back-folded across the DKP ring at the same time. It appears that repulsive interactions between the bulky aromatic groups favor the population of sterically less crowded conformations in the latter structure. In particular, a simultaneous population of the **F** rotamer by both side chains appears less probable.

Fig. 2. Extracts of long-term molecular-dynamics simulations for **2** (Langevin dynamics; implicit-solvent model for ACN): (*a*) time variation of the inter-side-chain distance *d*(O–O) between the tyrosine (Tyr) hydroxylic oxygen atom and the 4-benzoyl-phenylalanine (bpa) carbonyl oxygen atom; (*b*) time variation of the bpa side-chain dihedral angle; (*c*) time variation of the Tyr side-chain dihedral angle.

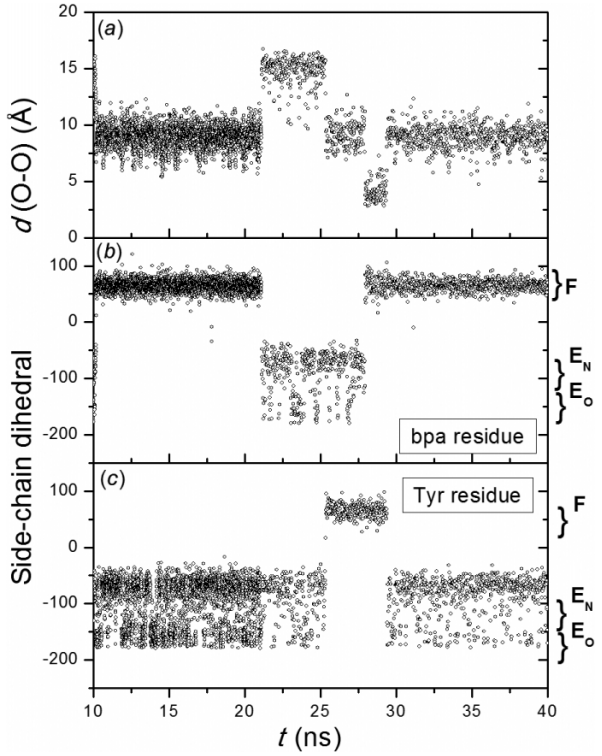

Conformational dynamics

The interconversion between different molecular conformations has been studied by means of long-term molecular-dynamics simulations (100 ns duration; implicit-solvent model for ACN). Figure 2 summarizes the time variation of 3 molecular parameters (both side-chain dihedral angles and the characteristic inter-side-chain distance) within a 30 ns simulation window for dyad **2**. In Fig. 2*a* the sum of the resident times at each distance (*d*(O–O)) should be viewed in regard to the total period of the simulation (100 ns); i.e., when the sums of these resident times are divided by the total time of the simulation, they basically reflect the relative existence of the dyad at each O–O distance (probability distribution). (Respective plots for **1** are given in the Supplementary data.)

In agreement with the NMR results, mainly 3 rotamers ($\mathbf{E_N}$, $\mathbf{E_O}$, and **F**) of each side chain are populated during the simulation of both compounds. Of particular interest was the probability of the **F–F** conformation of **2**, which allows for close contacts of <4.0 Å (Fig. 2) between the reacting moieties and closely resembles the quenching geometry of this dyad. As stated above, the simulations strongly disfavor this conformation: the calculated probability of the population of the **F–F** conformation is only 1.4%. In conclusion, the **F–F** conformation, although shown to be a rare conformation during the simulations for **2**, irrespective of the chosen starting geometry, is sufficient to explain the reactivity toward intramolecular HAT in the range of 10^7 s^{-1} (see further discussion).

As shown by DFT studies, close contacts of <3.2 Å within dyad **1** require the population of conformations that do not refer to side-chain rotamers. The formation of such structures does not appear at all during the 100 ns simulation (see Fig. S3 in the Supplementary data).

Laser flash photolysis: spectral and kinetic analyses

The excited-state dynamics of the dyads **1** and **2** were studied by means of nanosecond laser photolysis in 12 different solvents and solvent mixtures. Transient products were identified, and the efficiency of their formation was quantified by means of transient-absorption spectroscopy and spectral resolutions.

In all cases the triplet state was identified as the predominate intermediate in the early spectra by its characteristic absorption maxima at 325 nm (not shown) and 520 nm in addition to a long-wavelength absorption above 600 nm. The triplet state spectra of both dyads were indistinguishable and showed little variation with the change in solvent.

For bp∪Tyr dyads that are related to **1–2**, intramolecular HAT was found to be the predominate quenching pathway. The quantum yields for the formation of the respective biradicals were reported to be unity.[61] Thus, any significant spectral evolution with a spectral shift from 525 to 540 nm and accompanied by a growth at 405 nm would be indicative of the formation of ketyl and tyrosyl radicals, respectively. We found that the two dyads showed distinctly different spectral evolution during and after the decay of the triplet state.

This effect of the structure is illustrated by the transient spectra observed for solutions of **1** and **2** in ACN (Fig. 3). While the spectrum obtained for **1** in pure ACN after 200 ns largely resembles the original triplet spectrum, with its distinctive 520 nm absorption, the spectrum obtained for **2** carries significant contributions from a tyrosyl radical and a ketyl radical after only 100 ns. Note in particular the spectral shift of dyad **2** from the initial maximum of 520 nm to 540 nm, indicating the transition from its triplet to its ketyl radical. As shown in Fig. 3*b*, a change in the solvent did not significantly affect the transient absorption spectra of dyad **2**, an observation that holds for all of the studied solvents. Accordingly, deconvolution of the transient absorption spectra for compound **2** in an ACN–H_2O (2:1 *v*/*v*) mixture gave the same results as previously reported for pure ACN.[39] The quenching is found to proceed intramolecularly with high efficiency. This finding is in accordance with the lack of a concentration dependence of the triplet decay rate constants (see below). However, the intermediate (biradical) decays on the same time scale as it is formed. This behavior interferes with biradical accumulation and is contrary to the general observation that biradicals decay on a much longer time scale than do their parent triplets.[12,16,19,61]

In contrast to the largely solvent-independent behavior of **2**, the evolution of the transient spectra of dyad **1** is strongly dependent on the nature of the solvent. In particular, the spectrum obtained after 200 ns in the ACN–H_2O (2:1 *v*/*v*) mixture differs dramatically from the one in pure ACN and is fully consistent with efficient formation of ketyl and tyrosyl radicals. To clarify the nature of this solvent effect, the

Fig. 3. Transient absorption spectra obtained during laser flash photolysis at 355 nm of deoxygenated solutions (9×10^{-4} mol L^{-1}) of (*a*) compound **1** with a time delay of 200 ns and (*b*) compound **2** with a time delay of 100 ns; measurements in ACN (filled symbols) and in ACN–H_2O (2:1 *v*/*v*) (open symbols).

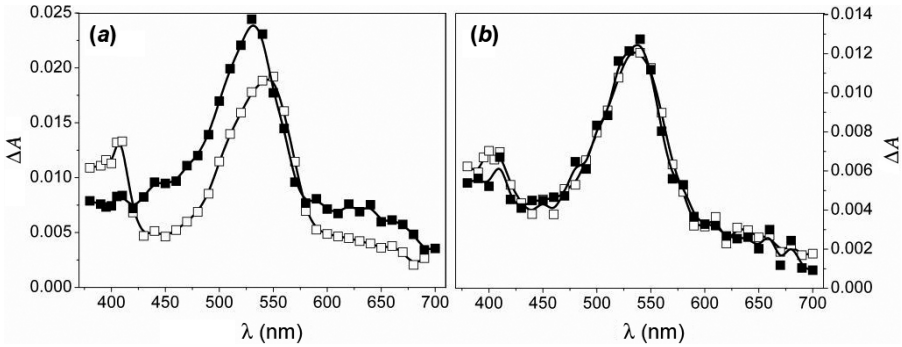

Fig. 4. (*a*) Resolutions of transient absorption spectra taken 1400 ns after 355 nm laser pulsing (5 mJ) of a solution of **1** in ACN. (*b*) Concentration profiles for the transients obtained from the deconvolution of transient absorption spectra of **1** in ACN. (*c*) Resolutions of transient absorption spectra taken 130 ns after 355 nm laser pulsing (5 mJ) of a solution of **1** in ACN–H_2O (1:1 *v*/*v*). (*d*) Concentration profiles for the transients obtained from the deconvolution of transient absorption spectra of **1** in ACN–H_2O (1:1 *v*/*v*). □, triplet state ^{3}bp; ○, ketyl radical bpH$^\bullet$; Δ, tyrosyl radical Tyr(O$^\bullet$); ◇, bp radical anion bp$^{\bullet-}$; *, experimental data. Solid curves are the resulting fits from the regression analysis.

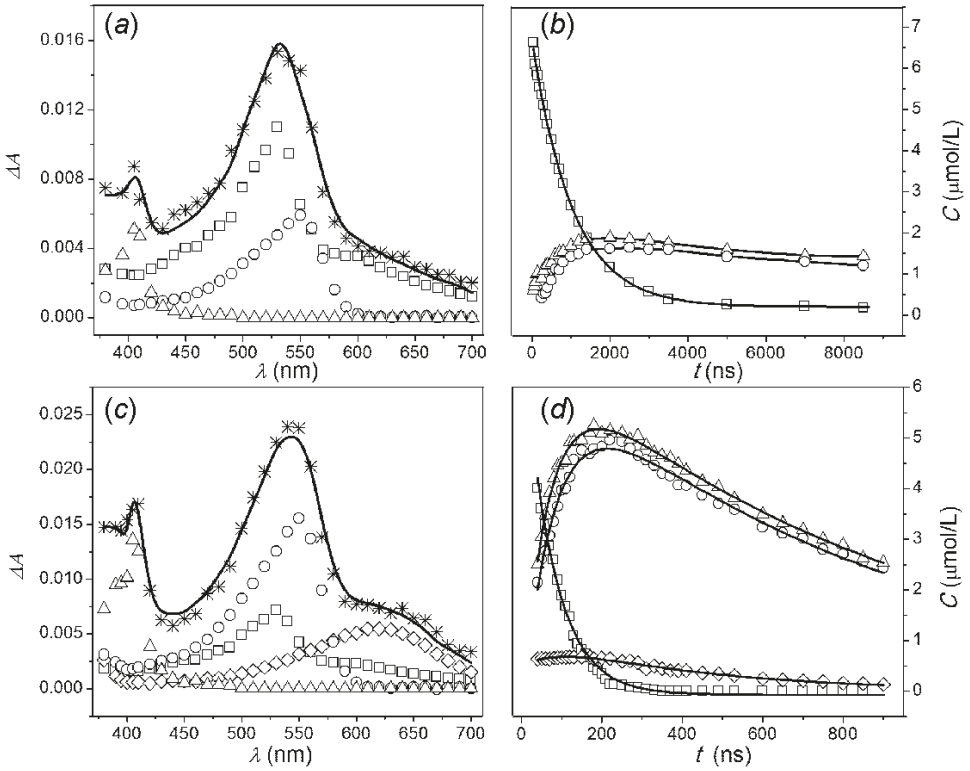

transient spectra obtained for compound **1** in ACN and ACN–H_2O (1:1 *v*/*v*) were deconvoluted into their spectral components, from which concentration–time profiles were constructed. Exemplary resolutions are given in Figs. 4*a* and 4*c* and the resulting profiles are displayed in Figs. 4*b* and 4*d*. These profiles reveal the distinct difference in the triplet quenching of dyad **1** in the two solvents. That is, the reaction is found to be intermolecular in ACN, whereas it is predominantly intramolecular in the ACN–H_2O (1:1 *v*/*v*) mixture. To simulate quantitatively the experimental data obtained in ACN for dyad **1**, only 3 components were needed: the triplet state ^{3}bp, ketyl radicals (bpH$^\bullet$), and tyrosyl radicals (Tyr(O$^\bullet$)) (see Fig. 4*a*). The concentrations of bpH$^\bullet$ and Tyr(O$^\bullet$) were found to be equal within the error estimation. The triplet decay obtained from the concentration profile is 1 μs, which is well in agreement with the triplet lifetime obtained from the kinetic traces at 630 nm. From the decomposition of the transient absorption spectra and the resulting concentration profile, the quantum yield for the formation of both radicals was calculated to be equal to 25% in ACN. Based on the long lifetimes of the radicals, which are decaying for tens of microseconds, we can conclude that they are formed mainly in self-quenching reactions (see Scheme 3).

Scheme 3. Deactivation paths (red, bimolecular; blue, unimolecular) of the triplet-excited state of the dyads **1** and **2**.

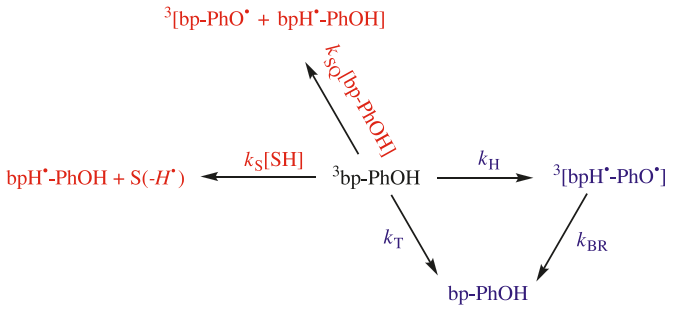

A totally different situation was observed for dyad **1** in ACN–H_2O (1:1 *v*/*v*). First, the triplet lifetime was reduced by a factor of 10. Second, to reproduce the experimental data, 4 components had to be used, namely ^{3}bp, ketyl radicals (bpH$^\bullet$), bp radical anions (bp$^{\bullet-}$), and tyrosyl radicals (Tyr(O$^\bullet$)). The rates of formation of the radical species bpH$^\bullet$, bp$^{\bullet-}$, and Tyr(O$^\bullet$) were, within experimental error, identical to the triplet-decay rate of dyad **1**. The total amount of bpH$^\bullet$ and bp$^{\bullet-}$ together was equal to the Tyr(O$^\bullet$) concentration, within experimental error. Formation and decay of both the ketyl radical and the tyrosyl radical appear to follow the same decay law. This is in accordance with an intramolecular reaction mechanism. The initial triplet concentration, after extrapolation to the end of the pulse, was 7.1 μmol L^{-1}. The maximum concentration of the tyrosyl radical was determined to be 6.9 μmol L^{-1}. This value was obtained from fitting the Tyr(O$^\bullet$) concentration profile to a function that takes into account the growth and the decay of the species. From this value and the above triplet concentration (actinometer), the quantum yield of the tyrosyl radical is seen to be close to unity. The same procedure was applied to the bp radical anion, and its quantum yield of formation was estimated to be 0.18. The results proved that not only can dyad **1** (which has the benzophenone and phenol moieties on opposite sides of the DKP ring) undergo intramolecular HAT, but this reaction can occur with quantum yields close to unity. Analogous behavior has been observed in other solvents such as ACN–H_2O mixtures, 2,2,2-trifluoroethanol (TFE), and 1,1,1,2,2,2-hexafluoropropanol (HFIP), except that the bp radical anion was detected only in ACN–H_2O mixtures.

The steering effects of the solvents on the efficiency of the intramolecular triplet quenching of dyads **1** and **2** manifest themselves also in the triplet lifetimes, which exhibit a remarkably distinct influence of the solvents. Some exemplary kinetic profiles, recorded at 630 nm, that illustrate the distinct solvent dependencies of the triplet decays of **1** and **2** are given in Fig. 5. For dyad **2**, where the benzophenone and tyrosine moieties occupy the same side of the DKP ring, the kinetic profiles coincide with each other, irrespective of the solvent. This indicates little impact of the solvent on the triplet lifetimes. Contrasting behavior was seen in dyad **1**, where the triplet lifetimes were very sensitive to the solvents and varied between approx. 50 ns in HFIP and >1000 ns in ACN or EtOAc. In general, the triplet lifetimes of **1** are reduced dramatically on going from non-protic to protic solvents. Thus, in contrast to the previous study of a pair of open-chain epimeric dyads, the triplet lifetimes of the two cyclic structures studied here exhibit completely distinct solvent dependencies.

To study the solvent effects on the intramolecular HAT pathway, the corresponding rate constants, k_H, have been isolated from the observed gross triplet-decay rate constants, k_{obs}. The latter have been extracted from the decay profiles at 630 nm (mono-exponential fits), the decay profiles at 520 nm (bi-exponential fits), and, in some cases, the triplet component of the concentration profiles (as in Figs. 4*b* and 4*d*; mono-exponential fits). Agreement between these methods was within 5%. The absolute value of the triplet-decay rate constant, k_{obs}, is the sum of the rate constants of the individual decay processes (Scheme 3). The evaluation procedures take into account (*i*) the solvent dependence of the intrinsic triplet lifetime of the bp chromophore by referencing it to the behavior of unsubstituted bp in the respective solvent and (*ii*) the effects of self-quenching (see Supplementary data). Due to the low laser power, effects of triplet–triplet annihilation were negligible.

A detailed kinetics data evaluation and a description of the way that we dealt with competition between intra- and intermolecular quenching paths can be found in the Supplementary data.

While the triplet decay of dyad **2** exhibited no significant concentration dependence, LFP results for dyad **1** in non-protic solvents, such as ACN or dichloromethane, show that the values for k_{obs} were concentration dependent. This behavior is due to contributions to bimolecular quenching from self-quenching, which leads to the ketyl radical and the tyrosyl radical with the rate constant k_{SQ}. The latter species decayed by bimolecular processes within tens of microseconds and therefore gave a virtually constant offset in the transient spectra on the time scale of the experiment. The self-quenching process was efficient in non-protic solvents where the reactivity toward intramolecular HAT was small. Notably, the k_H calculated from experiments at different concentrations, 2×10^{-5} mol L^{-1} (λ_{exc} = 266 nm) or 9×10^{-4} mol L^{-1} (λ_{exc} = 337 nm), were in a good agreement (Table 2).

The rate constants for the intramolecular HAT, k_H, calculated for dyad **1** range from $<1 \times 10^5$ s^{-1} in EtOAc to 2×10^7 s^{-1} in HFIP (see Table 2). The rate constants for the intramolecular HAT for dyad **2** varied only from 2.2×10^7 s^{-1} in ACN to 8.2×10^6 s^{-1} in TFE. The uncertainty in the rate constant values derived in this manner increases significantly with H-abstraction contributions from the solvent.

The results presented in Table 2 show a striking contrast between the two diastereomers with regard to the dependence of their k_H on solvent. The results show that a change in the configuration of just one chiral center produced completely distinct changes in the reactivity of the intramolecular HAT with a change in the solvent. The reaction rates for dyad **1** were found to be strongly solvent dependent, while the solvent was found to be of minor importance for the reaction rates of dyad **2**.

This contrasting solvent behavior toward the intramolecular HAT observed in **1** and **2** is unusual for a pair of diastereomers. In this regard they are found to be a unique pair of diastereomers with a unique solvent dependence of the

Fig. 5. Normalized decay profiles observed at 630 nm and mono-exponential fits to the decays for solutions of dyads **1** (*a*) and **2** (*b*). a, ethyl acetate; b, ACN; c, ACN–H_2O (2:1 *v*/*v*); d, trifluoroethanol.

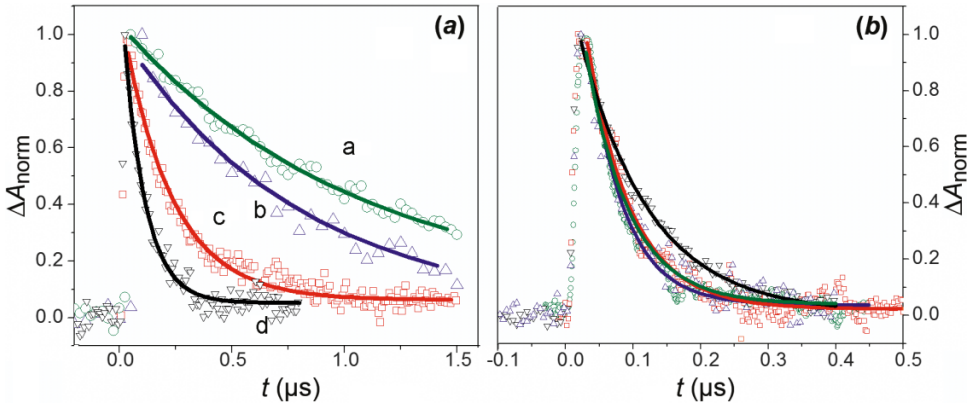

Table 2. Summary of solvent parameters and the kinetic data of dyads **1** and **2**.

		Solvent parameters			Rate constants		
	Solvent	$\Sigma\alpha_2^{H}$[a]	$\Sigma\beta_2^{H}$[a]	η[b]	k_H (**1**)[c]	k_H (**2**)[c]	S[d]
1	Chloroform	0.15	0.02	0.537	(2.2)	(11.5)	5.2
2	Dichloromethane	0.1	0.05	0.437	1.9 (2.0)	(14.5)	7.2
3	1,2-Dichloroethane	0.1	0.11	0.77	(1.7)	(13.6)	10.7
4	Acetonitrile	0.07	0.32	0.37	*0.3 (0.3)*	20.7 (20.0)	73.7
5	Benzonitrile	0	0.33	1.2	*0.3*	9.5	31.6
6	Ethyl acetate	0.0	0.45	0.423	*0.1*	14.4	131
7	Trifluoroethanol	0.57	0.25	1.8[e]	8.5	8.2	0.97
8	Methanol	0.43	0.47	0.544	*2.3 (2.8)*	*9.2*	3.9
9	Hexafluoro-2-propanol	0.77	0.10	1.02	21.1	15.7	0.74
10a	Acetonitrile/H_2O (9:1 *v*/*v*)	0.55[f]	≈0.34[g]	—	3.0	—	—
10b	Acetonitrile/H_2O (4:1 *v*/*v*)	0.61[f]	≈0.34[g]	—	5.5	—	—
10c	Acetonitrile/H_2O (2:1 *v*/*v*)	0.62[f]	≈0.34[g]	—	8.4	13.9	1.7

[a]Taken from ref. 67.

[b]At 25 °C (ref. 68).

[c]Results from 355 nm and 337 nm LFP (10^6 s^{-1}); experimental error ±5%, 0.7 mmol/L ≤ [**1**], [**2**] ≤ 2.6 mmol/L. Data in italics: experimental error ±20%. Data in parentheses from 266 nm LFP, 20 μmol/L ≤ [**1**], [**2**] ≤ 40 μmol/L.

[d]$S = k_H$ (**2**) / k_H (**1**).

[e]Taken from ref. 69.

[f]Interpolated from data in ref. 70.

[g]Linear interpolation from data in pure solvents, weighted by molar fractions.

stereoselectivity. Both epimers showed reactivity with respect to intramolecular HAT, but with a remarkable chiral discrimination in their rate constants, and this chiral discrimination strongly depends on the solvents. We and others previously reported stereoselection in HAT rates of diastereomeric ketone–phenol dyads in the range of 2–10 when expressed as the ratio of the rate constants of the intramolecular HAT between remote phenol and ketone moieties of these compounds.[16,19,29] The stereoselectivity ($S = k_H$ (**2**) / k_H (**1**)) found in this work varied from 131 to 0.74 (Table 2). In particular, the epimers revealed marked stereoselectivity in some of the non-protic solvents such as EtOAc and benzonitrile, much higher than has ever been reported previously. Quite unexpectedly, the stereoselectivity was significantly reduced in protic solvents. At extremes, compound **1**, which has the reactive moieties on opposite sides of the DKP ring, became more reactive than **2** in hexafluoro-2-propanol as a medium.

Discussion

In this study the excited-state dynamics of **1** and **2** have been taken as probes of structural effects on the efficiencies and rates of intramolecular hydrogen-atom transfer reactions. We find that the distinct steric constraints of the dyads, as outlined above, are reflected in distinct dynamics of the dyads' triplet states. The dyads particularly differ in their dependencies on the medium, as discussed below.

The intramolecular HAT in dyad **1** was found to be strongly solvent dependent, with the rate constants, k_H, ranging from $<1 \times 10^5$ s^{-1} to 2×10^7 s^{-1}. We recently observed a similar range of rate constants for the intramolecular HAT in one open-chain bp∪Tyr dyad,[30] whereas the HAT reactions in the open-chain congeners of **1** and **2** in a given solvent are generally faster by one to two orders of magnitude.[29] Such solvent-driven modulations of bimolecular HAT reaction rates of phenols have been generally attributed to effects of specific solvation of the phenol, which

Fig. 6. (*a*) Plot of H-atom transfer rate constants, $\log k_H$, against Abraham's effective H-bond acceptor ability (refs. 71, 73), $\Sigma\beta_2^H$, for protic solvents (open symbols) and non-protic solvents (filled symbols); (*b*) plot of H-atom transfer rate constants, $\log k_H$, against Abraham's effective H-bond donor ability (refs. 71, 73), $\Sigma\alpha_2^H$, for solvents with $\Sigma\beta_2^H \geq 0.25$ (filled symbols) and solvents with $\Sigma\beta_2^H \leq 0.11$ (open symbols); red symbols represent data for the **1**-(D,L) epimer and blue symbols represent data for the **2**-(L,L) epimer. (*c*) Semilogarithmic plot of stereoselectivity of H-atom transfer in dyads **1** and **2** as a function of the solvents' H-bond acceptor ability; open symbols represent protic solvents. (*d*) Semilogarithmic plot of stereoselectivity of H-atom transfer in dyads **1** and **2** as a function of the solvents' H-bond donor ability; open symbols represent solvents with $\Sigma\beta_2^H \leq 0.11$. Solvent codes as in Table 2.

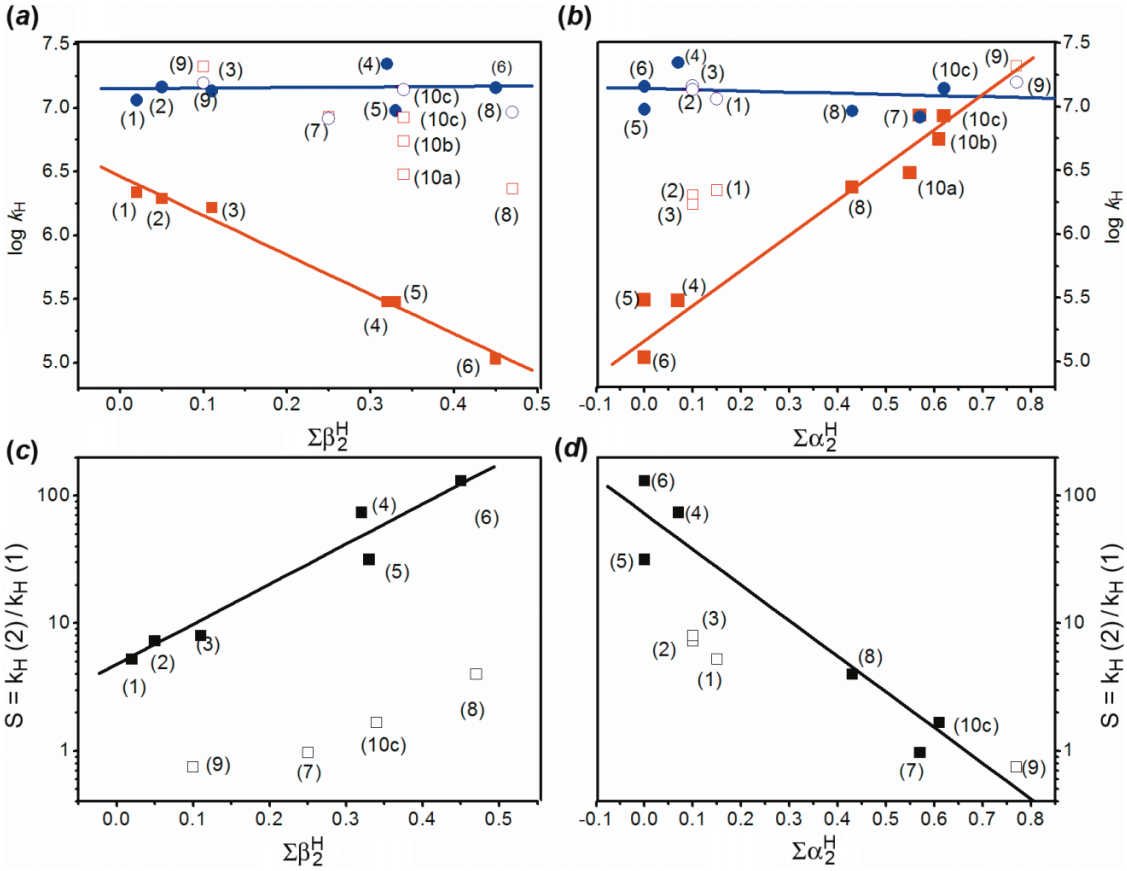

were coined as kinetic solvent effects. In particular, the previous work on the bimolecular HAT of phenols has shown that rate constants are correlated with the solvents' hydrogen-bond acceptor ability.[31–36,71,72] That is, the logarithmic rate constants depended linearly on a single solvent parameter, namely Abraham's H-bond acceptor ability,[71,73] irrespective of the molecularity of the reaction.[29] Notably, the solvent dependence cannot be fully explained by solute–solvent interactions of the tyrosine moiety. As shown here, the single-parameter dependence of the intramolecular HAT reaction that sufficed to explain the reactivity of the open-chain congeners of **1** and **2**[29] is not sufficient to explain the difference in reaction rate constants of the cyclic dyad **1**. Our results show that, in contrast to the phenomenology of the kinetic solvent effect, which necessarily connects specific solvation with reaction hindrance, specific solvation can also promote the HAT reactions of phenols.

In the following discussion the focus will first be on the data for dyad **1** displayed in Figs. 6*a* and 6*b* (red symbols).

A plot of the kinetic data for dyad **1** from Table 2 against the effective H-bond acceptor ability of the solvents (Fig. 6*a*) exhibits two different regions that reflect the character of the solvents. HAT rates in non-protic solvents with weak effective H-bond donor abilities, $\Sigma\alpha_2^H$ (red filled symbols in Fig. 6*a*), have a linear dependence on $\Sigma\beta_2^H$, with a slope $b = -3.1$ ($r^2 = 0.995$) and an intercept of 6.5. Thus, this dyad is another example where the slopes of the logarithmic intramolecular HAT rate constants versus $\Sigma\beta_2^H$ plots are characteristic for each dyad but not characteristic for each donor.[29,30]

The second region in Fig. 6*a* is that formed by the protic solvents with significant H-bond donor abilities. The protic solvents seem to allow much higher rate constants than their non-protic counterparts having similar H-bond acceptor abilities (nearly matching $\Sigma\beta_2^H$). For example, ethyl acetate and MeOH have almost the same H-bond acceptor ability, but k_H values for **1** differ by a factor of 10. Another example is the contrasting behavior of pure ACN and the ACN–H_2O (2:1 *v*/*v*) mixture, in which k_H values for **1** differ by a factor of 25. The large increase in the intramolecular HAT rate constant in protic solvents might be due to a switch in the mechanism.

The decrease of the HAT rates with the H-bond acceptor ability of the non-protic solvents suggests that negligible intramolecular reactivity is expected for dyad **1** in solvents with $\Sigma\beta_2^H > 0.3$. However, the data in Table 2 show that

protic solvents with high $\Sigma\beta_2^H$ values show significant reactivity for dyad **1**. In Fig. 6*b*, data from Table 2 are plotted against $\Sigma\alpha_2^H$; with the exception of the chlorohydrocarbons, there is a linear correlation for dyad **1** with a positive slope of 2.3 ($r^2 = 0.977$) and an intercept of 5.2. That is, the reactivity increases with the strength of the solvent–solute interaction.

In summary, opposite effects were exerted by non-protic and protic solvents on intramolecular HAT in dyad **1**. The relevant solvent parameters favoring efficient intramolecular HAT for dyad **1** are the solvents' small $\Sigma\beta_2^H$ values and high $\Sigma\alpha_2^H$ values. This was realized by HFIP, for example. The opposite behavior was seen in the poor reactivity in EtOAc, which can be explained on the basis of its high $\Sigma\beta_2^H$ (0.45) and low $\Sigma\alpha_2^H$ (0.00).

In conclusion, the solvent dependence of the cyclic dyad **1** sharply diverges from the behavior of its open-chain congener[29] but largely coincides with the phenomenology observed recently for a more rigid open-chain dyad.[30] Obviously, the observed phenomenology of the kinetic solvent effects reflects structural parameters of the dyads. This is most evident from the behavior of the cyclic dyad **2**, which lacks any significant dependence on the H-bonding properties of the solvent.

The plot of the logarithmic rate constants versus $\Sigma\beta_2^H$ for dyad **2** exibits no significant variance with the solvents' H-bond accepting or H-bond donating properties (blue symbols in Figs. 6*a* and 6*b*). Actually, the slopes are close to zero in both cases, which means that the rate constants for HAT for dyad **2** are independent of these parameters. Accordingly, the stereoselectivity of the HAT in **1** and **2**, expressed as the ratio of the rate constants and shown in Figs. 6*c* and 6*d*, directly reflects the solvent dependence of the HAT of **1**. The sharp decrease of the HAT reaction rates for dyad **1** in non-protic solvents with hydrogen-bond acceptor tendencies and, on the other hand, the sharp increase of the reaction rates in protic solvents with hydrogen-bond donor tendencies are the dominant sources of the solvent dependence of the stereoselectivity (Figs. 6*c* and 6*d*). Our findings are in contrast with other results where the stereoselectivity of the HAT process was solely dependent on the $\Sigma\beta_2^H$, irrespective of the protic or non-protic character of the solvents.

In conclusion, we have studied the behavior of the two cyclic-bridged dyads **1** and **2** in 12 different solvents and mixtures. It was shown that the properties of a solvent, i.e., its ability to act as a hydrogen bond donor or acceptor, play an important role in determining the HAT rate constants in only one of the two epimers in this study.

The contrasting solvent dependencies of the HAT rate constants for dyad **1** in protic and non-protic solvents can be interpreted as being due to fundamentally different HAT mechanisms in the respective solvents. In favor of this interpretation are the significant enhancement of the reaction rates in protic solvents and the presence of the bp radical anion in an ACN–H_2O (1:1 *v*/*v*) mixture. In addition, it is important to note that the intercepts of the single-solvent parameter regressions in Figs. 6*a* and 6*b* (red lines) differ by almost 2 orders of magnitude. These values represent the isolated and solvent-independent HAT rate constants and, thus, they should not vary if there is only a single common mechanism of HAT in protic and non-protic solvents.[30]

Moreover, NMR, molecular-dynamics simulations, and DFT results[39] have shown that conformations with extremely long distances (12.8 Å) between the reactive moieties are the most favorable ones in solution (Fig. 1; Table 1). The HAT rates in non-protic solvents are limited by the accessibility of free (i.e., not H-bonded) tyrosine. In contrast, the kinetic data obtained in protic media show a correlation between HAT rates and the H-bond donor ability of the solvent. Thus, at least for intramolecular HAT reactions, the solvation of the abstracting species should be considered, a priori, as important as the solvation of the H-donating species. However, the action of the protic solvent in this case and its impact on the mechanism of the HAT step remain under discussion and are the subject of further work.

Several pieces of evidence favor electron transfer involving pathways that are driven by specific H-bonding interactions of the electron acceptor with the protic solvent. An electron-transfer pathway in protic solvents has been observed recently for a sterically restricted bp∪TyrOH dyad. In this structure, the directionality of the benzamide linker of the dyad effectively excludes close intramolecular contacts. Studies of the solvent effects on the nanosecond-transient dynamics and on the chemically induced dynamic nuclear polarization following LFP have shown that in protic solvents the H abstraction reaction is initiated by electron transfer (G. Hörner and colleagues, unpublished data). Similar conclusions have been drawn from studies of the bimolecular electron transfer between anisole and ^{3}bp, where dramatic activating effects of strongly H-bonding solvents on the one-electron oxidation of anisole by ^{3}bp show that this phenomenon is not limited to phenols and might be of general significance.[74]

In contrast to the above discussion, neither of the rate-determining effects of solvation seems to be important for the HAT in dyad **2**, as there was little variation in the k_H rate constant among solvents. The ratio of the highest k_H obtained in ACN and the smallest k_H obtained in TFE is just 2.4 for the triplet state of dyad **2**. The absence of a marked solvent dependence, which was observed for all other dyads, therefore deserves further consideration. In particular, it raises the question, what are the factors determining the rate constants if there is no impact of specific solvation?

The observation that the triplet state of dyad **2** was quenched slightly more slowly in solvents with higher viscosity, which led to smaller values of k_H (TFE and benzonitrile, see Table 2), points to the importance of the intramolecular dynamics. Similar observations were made for its open-chain analogue.[29] The observation of a greatly diminished triplet reactivity of **2** in highly viscous *tert*-butanol further corroborates viscosity as another source of kinetic diversity. That is, the dynamics of the molecular motions bringing dyad **2** to its reactive state appear to be rate determining in all solvents, which implies that the intrinsic HAT reaction rate of the dyad, irrespective of its state of solvation, markedly exceeds the rates of the intramolecular motions.

To check whether molecular dynamics are the rate-determining steps of the intramolecular HAT of dyad **2**, we have estimated the rate constant for the formation of close-contact conformations, k_{OO}, based on the LD trajectories de-

scribed above. In the calculation of the relaxation time (τ_{rxn} from the integration in eq. [2]), we have neglected the negative values of $C_N(t)$, which occur for $t > 1.4$ ns, since they were becoming artificially large with increasing delay times. Neglecting these negative values of $C_N(t)$ means that our computed value of 0.4 ns for the relaxation time is an upper limit. The average fraction of conformations, $\langle N_{OO} \rangle$, with the O–O distance less than 4 Å was determined to be equal to 0.01. Using this value and the τ_{rxn} from eq. [2], the estimated value of k_{OO} was calculated to be $2.5 \pm 0.1 \times 10^7$ s^{-1} (from eq. [1]). The resulting good agreement between the rate constant of formation of close-contact conformations and the experimental value of the intramolecular HAT rate constant in ACN (see Table 2) indicates that intramolecular dynamics is the rate-determining step of the intramolecular HAT.

As discussed previously,[39] DFT calculations suggested the presence of a number of different conformers of **2** with nearly degenerate energies. In particular, calculations on dyad **2** in an ACN continuum highlighted the competition between a conformer with a short O–O distance (favorable for the quenching geometry) with other, more extended conformers of similar energy (but having unfavorable geometries for HAT). This situation has been put to the test in the current work using NMR studies and molecular-dynamics simulations. Taking into account the error in DFT calculations, we can state that the NMR data and the theoretical calculations are in quite good agreement. The NMR data and the simulations both show that conformers that allow for close contacts between the reacting centers have to overcome significant steric constraints.

While the energetic differences between all of the side-chain rotamers appear to be rather small according to the NMR data (<1.0 kcal mol^{-1}), other intrinsically non-reactive structures of dyad **2** with only one aromatic side chain folded over the DKP ring are certainly favored, as evident from NMR data and the simulations (Fig. 2). Thus, significant intramolecular rearrangements must precede the reaction and can even be rate determining as soon as the intrinsic HAT rate exceeds the rate of formation of the quenching geometry. This condition actually seems to hold for dyad **2**. As stressed before (see Fig. 2), the long-term dynamics simulations indicated that the formation of close-contact structures occurs for dyad **2**. In particular, the rate of this formation in an ACN continuum with $k_{OO} = 2.5 \pm 0.1 \times 10^7$ s^{-1} (computed from eqs. [1–3]) shows very good agreement with the observed rate constants of the HAT in this solvent (see Table 2).

Conclusions

In this work we addressed the solvent effects on unimolecular HAT reactions in two epimeric benzophenone–tyrosine dyads. In agreement with previous work,[29] effects of specific solvation as well as effects of the bulk viscosity have been identified as important controls of the intramolecular reactivity. Most interestingly, the limited intramolecular mobility imposed by the rigid peptide environment of the diketopiperazine spacer translates into a strongly contrasting phenomenology of the solvent effects between the two epimers. For the anti-configured epimer **1**, where both amino acid side chains occupy different half rooms of the diketopiperazine spacer, two solvent parameters influence the H abstraction rates, namely the effective H-bond acceptor ability, $\Sigma\beta_2^H$, and the effective H-bond donor ability, $\Sigma\alpha_2^H$, as defined by Abraham.[67] In sharp contrast, the syn-configured dyad **2** represents the first example for HAT reactions from a sterically unhindered phenol without any sizable dependence on specific solvation effects. The reciprocal dependence of the HAT rates of **2** on the bulk viscosity points to the intramolecular dynamics as the rate-determining step.

In conclusion, the presented experimental and theoretical work fully confirmed our hypothesis that the solvent-effect phenomenology of intramolecular HAT reactions of phenols is dependent on and correlated with the donor-acceptor geometry. Intramolecular HAT reactions from phenols yield kinetic solvent effects that are significantly correlated with structural features; that is, individual kinetic solvent effects are expected to prevail for every single system. This mechanistic feature will be put to the test in further work.

Supplementary data

Supplementary data for this article are available on the journal Web site (canjchem.nrc.ca).

Acknowledgements

Financial support from the Ministry of Science and Higher Education (Poland) (grant No. N204 143138) and from the Foundation for Polish Science is gratefully acknowledged. This work was supported by COST Chemistry CM0603. This is document No. NDRL 4851 from the Notre Dame Radiation Laboratory, which is supported by the Office of Basic Energy Sciences at the United States Department of Energy. The computation was supported by the Interdisciplinary Centre for Mathematical and Computational Modeling of Warsaw University (G28-21). A. L. is a scholar of Adam Mickiewicz University Foundation at 2010. A. L. thanks the Director of the Radiation Laboratory for a stipend that supported part of this work.

References

(1) Turro, N. J.; Ramamurth, V.; Scaiano, J. C. *Modern Molecular Photochemistry of Organic Molecules*; University Science Books: Sausalito, CA, 2010.
(2) Das, P. K.; Encinas, M. V.; Scaiano, J. C. *J. Am. Chem. Soc.* **1981**, *103* (14), 4154. doi:10.1021/ja00404a029.
(3) Biczók, L.; Berces, T.; Linschitz, H. *J. Am. Chem. Soc.* **1997**, *119* (45), 11071. doi:10.1021/ja972071c.
(4) Boate, D. R.; Johnston, L.; Scaiano, J. C. *Can. J. Chem.* **1989**, *67* (5), 927. doi:10.1139/v89-142.
(5) Canonica, S.; Hellrung, B.; Wirz, J. *J. Phys. Chem. A* **2000**, *104* (6), 1226. doi:10.1021/jp9930550.
(6) Cosa, G.; Scaiano, J. C. *Org. Biomol. Chem.* **2008**, *6* (24), 4609. doi:10.1039/b810765c. PMID:19039370.
(7) Galian, R. E.; Pastor-Perez, L.; Miranda, M. A.; Perez-Prieto, J. *Chem. Eur. J.* **2005**, *11* (11), 3443. doi:10.1002/chem.200401118.
(8) Galian, R. E.; Litwinienko, G.; Pérez-Prieto, J.; Ingold, K. U. *J. Am. Chem. Soc.* **2007**, *129* (30), 9280. doi:10.1021/ja071716y. PMID:17625849.
(9) Koner, A. L.; Pischel, U.; Nau, W. M. *Org. Lett.* **2007**, *9* (15), 2899. doi:10.1021/ol071165g. PMID:17580891.

(10) Lathioor, E. C.; Leigh, W. J. *Can. J. Chem.* **2001**, *79* (12), 1851. doi:10.1139/cjc-79-12-1851.
(11) Lathioor, E. C.; Leigh, W. J. *Photochem. Photobiol.* **2006**, *82* (1), 291. doi:10.1562/2005-06-20-RA-581. PMID: 16042506.
(12) Lathioor, E. C.; Leigh, W. J.; St. Pierre, M. J. *J. Am. Chem. Soc.* **1999**, *121* (51), 11984. doi:10.1021/ja991207z.
(13) Leigh, W. J.; Lathioor, E. C.; St. Pierre, M. J. *J. Am. Chem. Soc.* **1996**, *118* (49), 12339. doi:10.1021/ja961973v.
(14) Wakasa, M.; Hayashi, H. *J. Phys. Chem.* **1995**, *99* (47), 17074. doi:10.1021/j100047a004.
(15) Yamaji, M.; Aoyama, Y.; Furukawa, T.; Itoh, T.; Tobita, S. *Chem. Phys. Lett.* **2006**, *420* (1–3), 187. doi:10.1016/j.cplett. 2005.12.072.
(16) Miranda, M. A.; Lahoz, A.; Martınez-Manez, R.; Bosca, F.; Castell, J. V.; Perez-Prieto, J. *J. Am. Chem. Soc.* **1999**, *121* (49), 11569. doi:10.1021/ja990823s.
(17) Pérez-Prieto, J.; Boscá, F.; Galian, R. E.; Lahoz, A.; Domingo, L. R.; Miranda, M. A. *J. Org. Chem.* **2003**, *68* (13), 5104. doi:10.1021/jo034225e. PMID:12816463.
(18) Pérez-Prieto, J.; Galian, R. E.; Morant-Miñana, M. C.; Miranda, M. A. *Chem. Commun. (Camb.)* **2005**, (25): 3180. doi:10.1039/b500697j. PMID:15968364.
(19) Pérez-Prieto, J.; Lahoz, A.; Boscá, F.; Martinez-Mañez, R.; Miranda, M. A. *J. Org. Chem.* **2004**, *69* (2), 374. doi:10. 1021/jo0356199. PMID:14725449.
(20) Pérez-Prieto, J.; Stiriba, S. E.; Boscá, F.; Lahoz, A.; Domingo, L. R.; Mourabit, F.; Monti, S.; Miranda, M. A. *J. Org. Chem.* **2004**, *69* (25), 8618. doi:10.1021/jo048973v. PMID: 15575737.
(21) Pischel, U.; Nau, W. M. *Photochem. Photobiol. Sci.* **2002**, *1* (2), 141. doi:10.1039/b110108k. PMID:12659131.
(22) Pischel, U.; Patra, D.; Koner, A. L.; Nau, W. M. *Photochem. Photobiol.* **2006**, *82* (1), 310. doi:10.1562/2005-02-07-RA-434. PMID:15882091.
(23) Scaiano, J. C.; McGimpsey, W. G.; Leigh, W. J.; Jakobs, S. *J. Org. Chem.* **1987**, *52* (20), 4540. doi:10.1021/ jo00229a021.
(24) Seyedsayamdost, M. R.; Reece, S. Y.; Nocera, D. G.; Stubbe, J. *J. Am. Chem. Soc.* **2006**, *128* (5), 1569. doi:10. 1021/ja055926r. PMID:16448128.
(25) Sul'timova, N. B.; Levin, P. P.; Chaikovskayab, O. N. *Russ. Chem. Bull., Int. Ed.* **2005**, *56*, 1397.
(26) Yamaji, M.; Oshima, J.; Hidaka, M. *Chem. Phys. Lett.* **2009**, *475* (4–6), 235. doi:10.1016/j.cplett.2009.05.063.
(27) Stubbe, J.; van der Donk, W. A. *Chem. Rev.* **1998**, *98* (2), 705. doi:10.1021/cr9400875.
(28) Wagner, P. J.; Pabon, R.; Park, B. S.; Zand, A. R.; Ward, D. L. *J. Am. Chem. Soc.* **1994**, *116* (2), 589. doi:10.1021/ ja00081a020.
(29) Hörner, G.; Hug, G. L.; Lewandowska, A.; Kazmierczak, F.; Marciniak, B. *Chem. Eur. J.* **2009**, *15* (13), 3061. doi:10. 1002/chem.200802674.
(30) Hörner, G.; Lewandowska, A.; Hug, G. L.; Marciniak, B. *J. Phys. Chem. C* **2009**, *113* (27), 11695. doi:10.1021/ jp901740z.
(31) Avila, D. V.; Ingold, K. U.; Lusztyk, J.; Green, W. H.; Procopio, D. R. *J. Am. Chem. Soc.* **1995**, *117* (10), 2929. doi:10. 1021/ja00115a029.
(32) Banks, J. T.; Ingold, K. U.; Lusztyk, J. *J. Am. Chem. Soc.* **1996**, *118* (28), 6790. doi:10.1021/ja961032i.
(33) Litwinienko, G.; Ingold, K. U. *J. Org. Chem.* **2003**, *68* (9), 3433. doi:10.1021/jo026917t. PMID:12713343.
(34) Litwinienko, G.; Ingold, K. U. *J. Org. Chem.* **2004**, *69* (18), 5888. doi:10.1021/jo049254j. PMID:15373474.
(35) Litwinienko, G.; Ingold, K. U. *J. Org. Chem.* **2005**, *70* (22), 8982. doi:10.1021/jo051474p. PMID:16238337.
(36) Litwinienko, G.; Ingold, K. U. *Acc. Chem. Res.* **2007**, *40* (3), 222. doi:10.1021/ar0682029. PMID:17370994.
(37) Hug, G. L.; Bobrowski, K.; Pogocki, D.; Hörner, G.; Marciniak, B. *ChemPhysChem* **2007**, *8* (15), 2202. doi:10.1002/ cphc.200700369. PMID:17910022.
(38) Kopple, K. D.; Ohnishi, M. J. *J. Am. Chem. Soc.* **1969**, *91* (4), 962. doi:10.1021/ja01032a029. PMID:5778278.
(39) Lewandowska, A.; Hug, G. L.; Hörner, G.; Carmichael, I.; Kazmierczak, F.; Marciniak, B. *Chem. Phys. Lett.* **2009**, *473* (4–6), 348. doi:10.1016/j.cplett.2009.03.085.
(40) Kirby, G. W.; Michael, J. *J. Chem. Soc. Chem. Commun.* **1971**, *187*, 415.
(41) Nitecki, D. E.; Halpern, B.; Westley, J. W. *J. Org. Chem.* **1968**, *33* (2), 864. doi:10.1021/jo01266a091.
(42) Leach, A. R. *Molecular Modelling: Principles and Applications*; Longman: Harlow, England, 1996.
(43) Frenkel, D.; Smit, B. *Understanding Molecular Simulation. From Algorithms to Applications*; Academic Press: San Diego, 1996.
(44) Widmalm, G.; Pastor, R. W. *J. Chem. Soc., Faraday Trans.* **1992**, *88* (13), 1747. doi:10.1039/ft9928801747.
(45) Levy, R. M.; Karplus, M.; McCammon, J. A.. *Chem. Phys. Lett.* **1979**, *65* (1), 4. doi:10.1016/0009-2614(79)80114-1.
(46) He, S.; Scheraga, H. A. *J. Chem. Phys.* **1998**, *108* (1), 287. doi:10.1063/1.475379.
(47) Field, M. J. *A Practical Introduction to the Simulation of Molecular Systems*; Cambridge University Press: Cambridge, 1999.
(48) Hinchliffe, A. *Chemical Modeling. From Atoms to Liquids*; John Wiley & Sons: Chichester, UK, 1999.
(49) MacKarell, A. D., Jr.; Bashford, D.; Bellott, M.; Dunbrack, R. L., Jr.; Evanseck, J. D.; Field, M. J.; Fischer, S.; Gao, J.; Guo, H.; Ha, S.; Joseph-McCarthy, D.; Kuchnir, L.; Kuczera, K.; Lau, F. T. K.; Mattos, C.; Michnick, S.; Ngo, T.; Nguyen, D. T.; Prodhom, B.; Reiher, W. E., III; Roux, B.; Schlenkrich, M.; Smith, J. C.; Stote, R.; Straub, J.; Watanabe, M.; Wiórkiewicz-Kuczera, J.; Yin, D.; Karplus, M. *J. Phys. Chem. B* **1998**, *102* (18), 3586. doi:10.1021/jp973084f.
(50) Gasteiger, J.; Marsili, M. *Tetrahedron* **1980**, *36* (22), 3219. doi:10.1016/0040-4020(80)80168-2.
(51) Venable, R. M.; Zhang, Y.; Hardy, B. J.; Pastor, R. W. *Science* **1993**, *262* (5131), 223. doi:10.1126/science. 8211140. PMID:8211140.
(52) Hypercube. *HyperChem® Computational Chemistry*; Hypercube, Inc.: Gainesville, FL, 2002.
(53) Allen, M. P.; Tildesley, D. J. *Computer Simulation of Liquids*; Oxford University Press: New York, 1987.
(54) Pogocki, D.; Schöneich, C. *Chem. Res. Toxicol.* **2002**, *15* (3), 408. doi:10.1021/tx0101550. PMID:11896689.
(55) Chandler, D. *Introduction to Modern Statistical Mechanics*; Oxford University Press: Oxford, 1987.
(56) Zwanzig, R.; Ailawadi, N. K. *Phys. Rev.* **1969**, *182* (1), 280. doi:10.1103/PhysRev.182.280.
(57) Pedzinski, T.; Markiewicz, A.; Marciniak, B. *Res. Chem. Intermed.* **2009**, *35* (4), 497. doi:10.1007/s11164-009-0046-4.
(58) Thomas, M. D.; Hug, G. L. *Comput. Chem.* **1988**, *22* (6), 491. doi:10.1016/S0097-8485(98)00022-9.
(59) Ludwig, M.; Asher, S. A. *J. Am. Chem. Soc.* **1988**, *110* (4), 1005. doi:10.1021/ja00212a004.
(60) Laws, W. R.; Ross, J. B. A.; Wyssbrod, H. R.; Beechem, J.

M.; Brand, L.; Sutherland, J. C. *Biochemistry* **1986**, *25* (3), 599. doi:10.1021/bi00351a013.
(61) Hörner, G.; Hug, G. L.; Pogocki, D.; Filipiak, P.; Bauer, W.; Grohmann, A.; Lämmermann, A.; Pedzinski, T.; Marciniak, B. *Chem. Eur. J.* **2008**, *14* (26), 7913. doi:10.1002/chem.200800315.
(62) Kobayashi, J.; Higashijima, T.; Miyazawa, T. *Int. J. Pept. Protein Res.* **1984**, *24* (1), 40. doi:10.1111/j.1399-3011.1984.tb00925.x.
(63) Kobayashi, J.; Higashijima, T.; Sekido, S.; Miyazawa, T. *Int. J. Pept. Protein Res.* **1981**, *17* (4), 486. doi:10.1111/j.1399-3011.1981.tb02018.x.
(64) Kobayashi, J.; Nagai, U. *Biopolymers* **1978**, *17* (9), 2265. doi:10.1002/bip.1978.360170918.
(65) Donzel, B.; Gauduchon, P.; Wahl, Ph. *J. Am. Chem. Soc.* **1974**, *96* (3), 801. doi:10.1021/ja00810a027.
(66) Chandrasekaran, R.; Lakshminarayanan, A. V.; Mohanakrishnan, P.; Ramachandran, G. N. *Biopolymers* **1973**, *12* (6), 1421. doi:10.1002/bip.1973.360120615.
(67) Abraham, M. H. *Chem. Soc. Rev.* **1993**, *22* (2), 73. doi:10.1039/cs9932200073.
(68) *CRC Handbook of Chemistry and Physics*, 76th ed.; D. R. Lide (Ed.); CRC Press: Boca Raton, 1995.
(69) Sierra, P. S.; Tejuca, C. C.; Garcia-Blanca, F. *Helv. Chim. Acta* **2005**, *88*, 312.
(70) Marcus, Y.; Migron, Y. *J. Phys. Chem.* **1991**, *95*, 400.
(71) Snelgrove, D. W.; Lusztyk, J.; Banks, J. T.; Mulder, P.; Ingold, K. U. *J. Am. Chem. Soc.* **2001**, *123* (3), 469. doi:10.1021/ja002301e.
(72) Valgimigli, L.; Banks, J. T.; Ingold, K. U.; Lusztyk, J. *J. Am. Chem. Soc.* **1995**, *117* (40), 9966. doi:10.1021/ja00145a005.
(73) Abraham, M. H.; Grellier, P. L.; Prior, D. V.; Morris, J. J.; Taylor, P. J. *J. Chem. Soc., Dalton Trans.* **1990**, *20*, 521.
(74) Lewandowska, A.; Hug, G. L.; Hörner, G.; Pedzinski, T.; Filipiak, P.; Marciniak, B. *ChemPhysChem* **2010**, *11* (10), 2108. doi:10.1002/cphc.201000196. PMID:20540143.